Microchim Acta (2014) 181:775–781
DOI 10.1007/s00604-013-1073-9

ORIGINAL PAPER

Direct formation of mesoporous upconverting core-shell nanoparticles for bioimaging of living cells

Lining Sun · Tao Liu · Yannan Qiu · Jinliang Liu · Liyi Shi · Otto S. Wolfbeis

Received: 10 May 2013 / Accepted: 19 August 2013 / Published online: 8 September 2013

Abstract We have developed a one-step method for the synthesis of mesoporous upconverting nanoparticles (MUCNs) of the type $NaYF_4$:Yb,Er@$mSiO_2$ in ammoniacal ethanol/water solution. The mesoporous silica is directly encapsulating the hydrophobic upconversion nanoparticles (UCNs) due to the presence of the template CTAB. Intense green emission (between 520 and 560 nm) and weaker red emission (between 630 and 670 nm) is observed upon 980-nm laser excitation. The MUCNs display low cytotoxicity (as revealed by an MTT test) and were successfully applied to label and image human nasopharyngeal epidermal carcinoma (KB) cells.

Keywords Upconversion nanophosphor · Mesoporous silica · Core-shell · Luminescence imaging · Biocompatible nanoparticles

Introduction

Smart combinations of different types of functional nanostructured materials will facilitate the development of multifunctional nanomedical platforms for multimodal imaging or simultaneous theranostics [1, 2]. Lanthanide-doped upconversion nanoparticles (UCNs), which undergo anti-Stokes emission processes where the long-wavelength pump sources (typically 980 nm) are upconverted to short-wavelength luminescence ranging from the deep-UV to the near-infrared (NIR), have recently drawn much attention in fields as diverse as laser materials, solar cells, data storage and bioapplications [3–7]. In marked contrast to conventional Stokes-shifted fluorophores such as quantum dots (QDs), organic dyes or fluorescent proteins, UCNs excited by continuous-wave NIR multi-photons avoid any auto-fluorescence from biosamples, increase the penetration depth and minimize photo-damage to living organisms evoking wide applications in biological labeling, imaging and therapeutics [8–15].

Mesoporous silica-based nanocomposites (MSNs), such as CdSe/ZnS@$mSiO_2$ [16], Fe_3O_4@$mSiO_2$ [17, 18], and MnO@$mSiO_2$ [19], are ideal candidates for constructing multifunctional nanoplatforms since MSNs possess unique structural properties such as large surface area, uniform mesopores, good biocompatibility, and also can be easily chemically functionalized on their surface [1, 20]. Several methods have been developed to coat both hydrophilic and hydrophobic UCNs with mesoporous silica, constructing core-shell nanoparticles for photodynamic therapy (PDT) [21], drug delivery [22] and secondary excitation [23]. For example, a two-step silica-coating procedure was employed in which a thin layer of dense silica was firstly coated onto the UCNs to form UCNs@silica nanoparticles, which then acted as seeds for the growth of another layer of mesoporous silica to obtain final core-shell structures [22]. This method is, however relatively complicated and time consuming. Therefore, a general and simple strategy for offering surface meso-functionality is greatly welcomed to prepare biocompatible and uniform mesoporous upconverting nanocomposites [24–27].

Here, we present a facile one-step method for direct formation of core-shell mesoporous silica coated upconverting nanoparticles (MUCNs), $NaYF_4$:Yb,Er@$mSiO_2$, by using cetyltrimethylammonium bromide (CTAB) as both phase transfer assisting agents and pore-generating templates. To

Electronic supplementary material The online version of this article (doi:10.1007/s00604-013-1073-9) contains supplementary material, which is available to authorized users.

L. Sun (✉) · T. Liu · Y. Qiu · J. Liu · L. Shi (✉)
Research Center of Nano Science and Technology, Shanghai University, Shanghai 200444, People's Republic of China
e-mail: lnsun@shu.edu.cn
e-mail: shiliyi@shu.edu.cn

O. S. Wolfbeis
Institute of Analytical Chemistry, Chemo- and Biosensors, University of Regensburg, 93040 Regensburg, Germany

the best of our knowledge, this is the first time, in an ammonia and ethanol aqueous solution, to directly coat mesoporous silica onto the surface of hydrophobic UCNs synthesized by solvothermal method and the obtained MUCNs were successfully applied to in vitro bioimaging [28–30].

Experimental section

Chemical and reagents

All chemicals were used as received without further purification. NaOH, NH_4F, ethanol, methanol, cetyltrimethylammonium bromide (CTAB), cyclohexane, and acetone were purchased from Sinopharm Chemical Reagent Co., Ltd. Oleic acid was obtained from Alfa Aesar. 1-Octadecene, tetraethyl orthosilicate (TEOS), aqueous ammonia (28 %) were purchased from Aladin Company. $ErCl_3{\cdot}6H_2O$, $YbCl_3{\cdot}6H_2O$, $YCl_3{\cdot}6H_2O$ were purchased from Sigma Aldrich. Deionized water was used in the experiments throughout.

Synthesis of $NaYF_4$:Yb,Er (18/2 mol%) nanocrystal

$NaYF_4$:Yb,Er nanocrystals were synthesized following a protocol that was reported previously [31]. YCl_3 (0.8 mmol), $YbCl_3$ (0.18 mmol), and $ErCl_3$ (0.02 mmol) were mixed with 6 mL oleic acid and 15 mL 1-Octadecene (ODE) in a 100 mL flask. The solution was heated to 150 °C to form a homogeneous solution, and then cooled to room temperature. A 10 mL methanol solution containing NaOH (2.5 mmol) and NH_4F (4 mmol) was added into the flask and stirred for a while. The solution was slowly heated to remove methanol, degassed at 100 °C for 10 min, and then heated to 300 °C and maintained for 1 h under Argon protection. After the solution was cooled naturally, nanocrystals were precipitated from the solution with ethanol and washed with ethanol/cyclohexane (1:1 v/v) three times. Finally, the purified $NaYF_4$:Yb,Er nanocrystals were dispersed in 20 mL of cyclohexane.

Phase transfer from cyclohexane to water

Two milliliters of the UCNs solution (10 $\mu g{\cdot}mL^{-1}$) was mixed with 100 mg of CTAB and 20 mL of water. The mixture was then stirred vigorously for 3 h, and the formation of the oil-in-water micro-emulsion appeared with a transparent solution. Then the cyclohexane solvent was boiled off from the solution, resulting in a transparent UCNs&CTAB solution. The solution was filtered through a 0.45 μm syringe filter to remove any large aggregates or contaminants.

Formation of $NaYF_4$:Yb,Er@$mSiO_2$

After filtering, the UCNs&CTAB solution obtained was redispersed in a mixed solution containing 60 mL of water, 75 mL of ethanol, and 2 mL of aqueous ammonia (28 %). After the mixture was ultrasonicated for 1 h, 60 μL of TEOS dispersed in 5 mL of ethanol was added dropwise into the above mixture under ultrasonication. Then the mixture was heated to 70 °C and stirred for 18 h at speed of 700 rpm. The MUCNs were precipitated and washed with ethanol/water (1:1 v/v) several times and then MUCNs were dispersed in 20 mL of ethanol. To extract CTAB from the MUCNs, 40 μL of HCl was added to the dispersion (pH~1.43) and stirred for 3 h at 60 °C.

Cytotoxicity of MUCNs

In vitro cytotoxicity was measured by performing methyl thiazolyltetrazolium (MTT) assays on the human nasopharyngeal epidermal carcinoma cells (KB cells). Cells were seeded into a 96-well cell culture plate at 5×10^4/well, under 100 % humidity, and were cultured at 37 °C and 5 % CO_2 for 24 h; different concentrations of MUCNs (0, 100, 200, 300 and 400 $\mu g{\cdot}mL^{-1}$, diluted in RPMI 1640) were then added to the wells. The cells were subsequently incubated for 4 h and 24 h at 37 °C under 5 % CO_2. Thereafter, MTT (10 μL; 5 $\mu g{\cdot}mL^{-1}$) was added to each well and the plate was incubated for an additional 2 h at 37 °C under 5 % CO_2. After the addition of 100 μL DMSO, the assay plate was allowed to stand at room temperature for 2 h. The OD570 value (Abs.) of each well, with background subtraction at 690 nm, was measured by means of a Tecan Infinite M200 monochromator-based multifunction microplate reader.

The following formula was used to calculate the inhibition of cell growth[14]:

$$\text{Cell viability}(\%) = (\text{mean of Abs. value of treatment group}/\text{mean of Abs. value of control}) \times 100\%.$$

Laser scanning upconversion luminescence imaging

KB cells were plated on 14 mm glass coverslips and allowed to adhere for 24 h. Then KB cells were incubated in a serum-free medium containing 200 $\mu g{\cdot}mL^{-1}$ MUCNs for 1 h at 37 °C under 5 % CO_2. Subsequently, cell imaging was then carried out after washing the cells with PBS three times to remove the excess MUCNs. Confocal imaging of cells was performed with a modified Olympus FV1000 laser scanning upconversion luminescence microscope (LSUCLM) equipped with a continuous-wave (CW) laser at 980 nm (Connet Fiber Optics, China). A 40 × oil-immersion objective

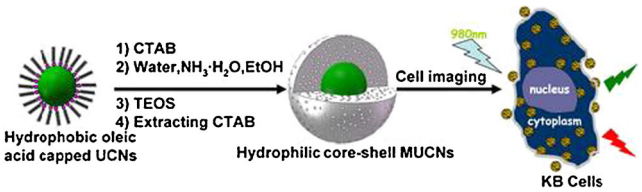

Scheme 1 Schematic illustration of the overall synthetic and cell imaging protocol

lens was used. For the MUCNs, the CW laser at 980 nm provided the excitation, and UCL emission was collected at the green (520–560 nm) and red (630–670 nm) channels.

Results and discussion

Scheme 1 illustrates the overall synthetic and bioimaging protocol of MUCNs. The oleate-capped $NaYF_4$:Yb,Er (18/2 mol%) UCNs (Fig. S1, ESI†) prepared via the solvothermal method show a uniform and monodisperse morphology (Fig. 1a) and have a diameter of approximately 50 nm with high crystallinity indicated from high-resolution TEM (inset of Fig. 1a).

The diffraction peaks' positions and intensities in XRD pattern (blue line in Fig. 2) can be attributed to the standard card of β-$NaYF_4$:Yb,Er (JCPDS 16-0334) (black line in Fig. 2) which are well known to be the most effective upconverter [32, 33]. Here, to obtain water-dispersible nanocrystals, the hydrophobic UCNs dispersed in cyclohexane were transferred to aqueous phase by mixing and vigorously stirring them with an CTAB aqueous solution followed by completely evaporating cyclohexane. The hydrophobic tail of the CTAB molecules interact strongly with the oleic acid ligands on the surface of the UCNs via van der Waals interactions and the hydrophilic headgroups of CTAB rendered the UCNs water-soluble [16]. As a result, a transparent solution was obtained (1 mg·mL^{-1}, Fig. S2, S3, ESI†) [34].

In the subsequent sol–gel reaction upon addition of tetraethylorthosilicate (TEOS), the silica/CTAB layer is formed around CTAB-stabilized nanocrystals under basic conditions through an electrostatic interaction between the cationic (CTAB) and anionic (silicate) species. The UCNs&CTAB

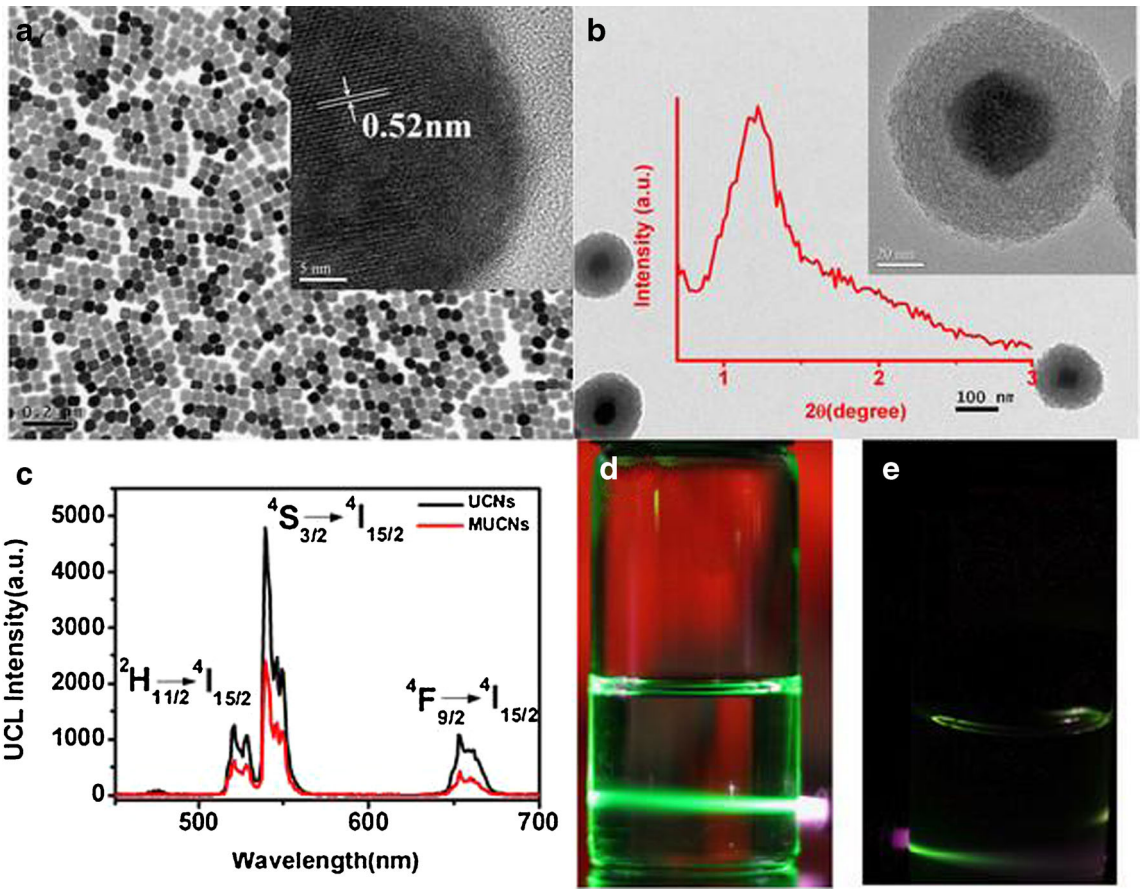

Fig. 1 TEM images of (**a**) UCNs and (**b**) MUCNs. (**c**) Upconversion luminescence spectra of UCNs (*black line*) and MUCNs (*red line*). Photographs of (**d**) UCNs in cyclohexane (1 mg·mL^{-1}) and (**e**) MUCNs in water (1 mg·mL^{-1}) under excitation of CW 980 nm light with a power of 1 W, respectively (insets in (**a**) and (**b**): HRTEM images of UCNs and MUCNs, respectively and low angle XRD pattern of MUCNs)

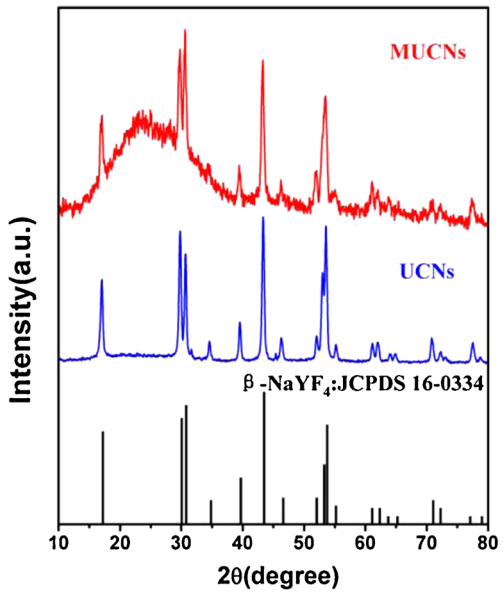

Fig. 2 XRD patterns of UCNs (*blue line*) and MUCNs (*red line*). The standard pattern of β-$NaYF_4$ has been given (*black line*) as a reference

nanoparticles (73.5 eV) directly act as seeds for the formation of spherical mesoporous silica shell by hydrolysis and condensation of TEOS [20]. Comparision with the two-step silica coating proecdure [21–23], in this case, the UCNs need not to be firstly coated a nonporous silica shell to facilitate the following mesoporous silica growth. The TEM image (Fig. 1b) reveals that MUCNs are spherical with core-shell structures, which shows uniform size and mono-dispersibility. Mesoporous shell with interconnected wormhole-like pores were clearly seen from the high-resolution TEM (inset in Fig. 1b). Combined with XRD pattern (red line) in Fig. 2 which shows a peak at 2θ=20° corresponding to silica, scanning transmission electron microscopy (STEM) and the corresponding EDX elemental mapping and spectra in Fig. 3, the formation of core-shell structures is further corroborated by indicating the presence of the elements Si, F, Y, and Yb (Due to the low Yb doping concentration, the magnified image of the Yb element mapping image is displayed in Fig. S4., ESI†) in the MUCNs. As shown in Fig. 1b (inset), the low-angle XRD pattern of the mesoporous nanospheres also showed a two-dimensional (2D) short-range ordered mesostructure of the shell component. In addition, the N_2 adsorption/desorption isotherms classified as type-IV further demonstrate the mesoporous characteristics of MUCNs. The corresponding Barrett–Joiner–Halenda (BJH) pore size distribution demonstrated that the mean mesoporous size of the MUCNs is 2.26 nm and the Brunauer–Emmett–Teller (BET) surface area and the total pore volume were calculated to be 55.97 $m^2 \cdot g^{-1}$ and 0.2951 $cm^3 \cdot g^{-1}$, respectively.

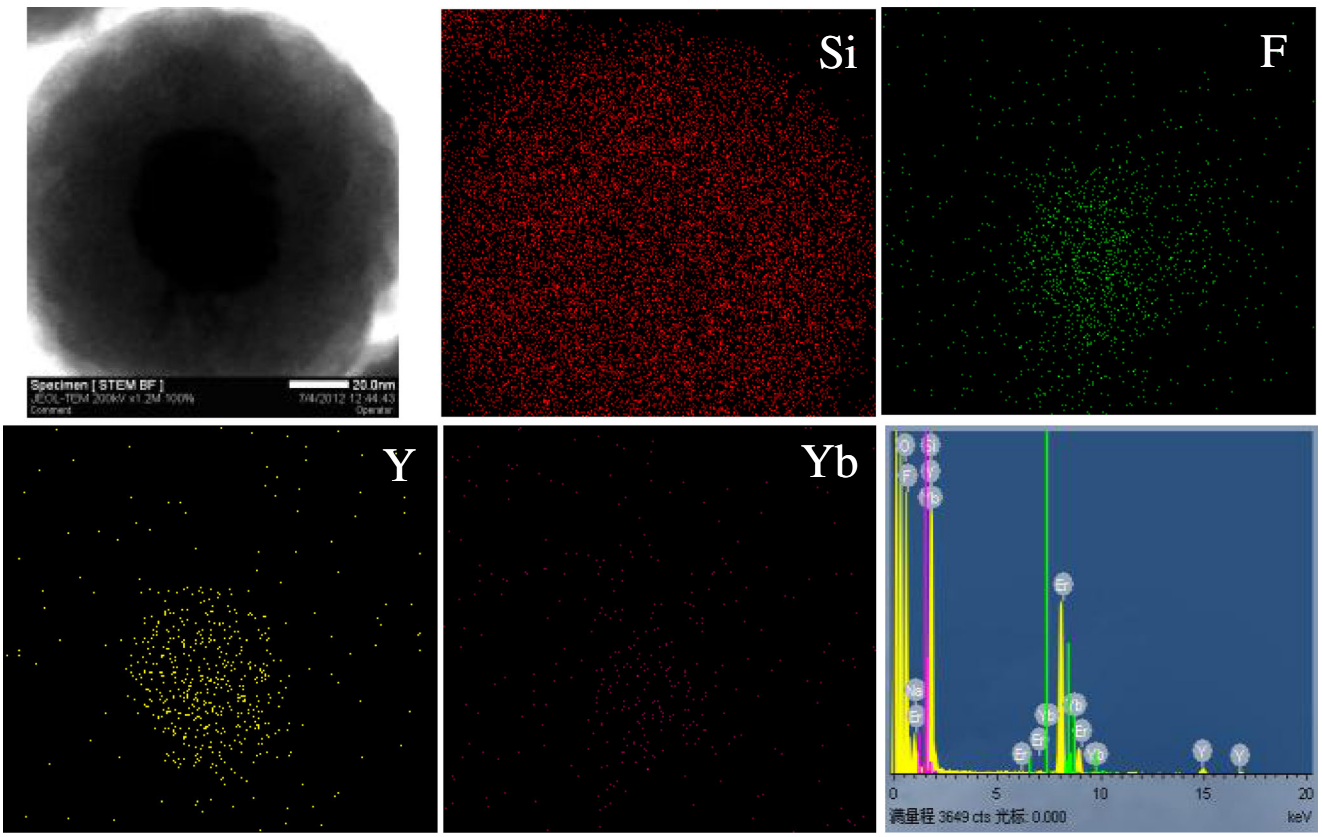

Fig. 3 Scanning transmission electron microscopy image, EDX elemental mapping, and spectra of mesoporous upconverting nanoparticles

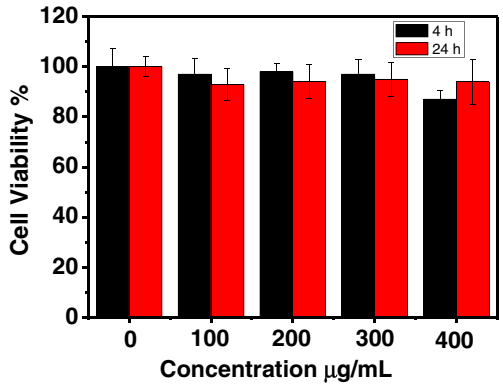

Fig. 4 In vitro cell viability of KB cells incubated with MUCNs at different concentrations for 4 h (*black*) and 24 h (*red*), respectively

In order to assess the feasibility of $NaYF_4$:Yb,Er@$mSiO_2$ for upconversion luminescent (UCL) bioimaging, the UCL spectra under CW 980 nm light excitation of transparent colloidal solutions of $NaYF_4$:Yb,Er nanocrystals in cyclohexane and $NaYF_4$:Yb,Er@$mSiO_2$ nanospheres in water are initially shown in Fig. 1c. The well-known emission peaks of UCNs at 521, 539, and 651 nm can be ascribed to the transitions from the energy levels $^4H_{11/2}$, $^4S_{3/2}$, and $^4F_{9/2}$ to the ground state $^4I_{15/2}$ of Er^{3+} ion, respectively [35]. No obvious change in the UCL wavelength and sharpness except a slight decrease in luminescence intensity (Fig. 1d and e) was observed after meso-functionalization.

Encouraged by the effective emission of candidate imaging agents $NaYF_4$:Yb,Er@$mSiO_2$, we conducted in vitro bioimaging experiment. Before the MUCNs were used as bioprobes, however, it is critical to investigate the cytotoxicity and cell-permeability characteristics of these nanoparticles with the methyl thiazolyltetrazolium (MTT) assay. Upon incubation with the MUCNs over a range of dosages (0–400 $\mu g \cdot mL^{-1}$), as illustrated in Fig. 4, even at higher concentrations (400 $\mu g \cdot mL^{-1}$), KB cell viability still remained at above 85 %. It can be observed that the KB cell viability for 24 h is higher than that for 4 h with 400 μg/mL MUCNs, which is within experimental error of the MTT measurements. On the basis of the MTT assay results, it can be inferred that the MUCNs are biocompatible and nearly nontoxic to live cells and thus can serve as safe luminescent bioprobes [30, 36].

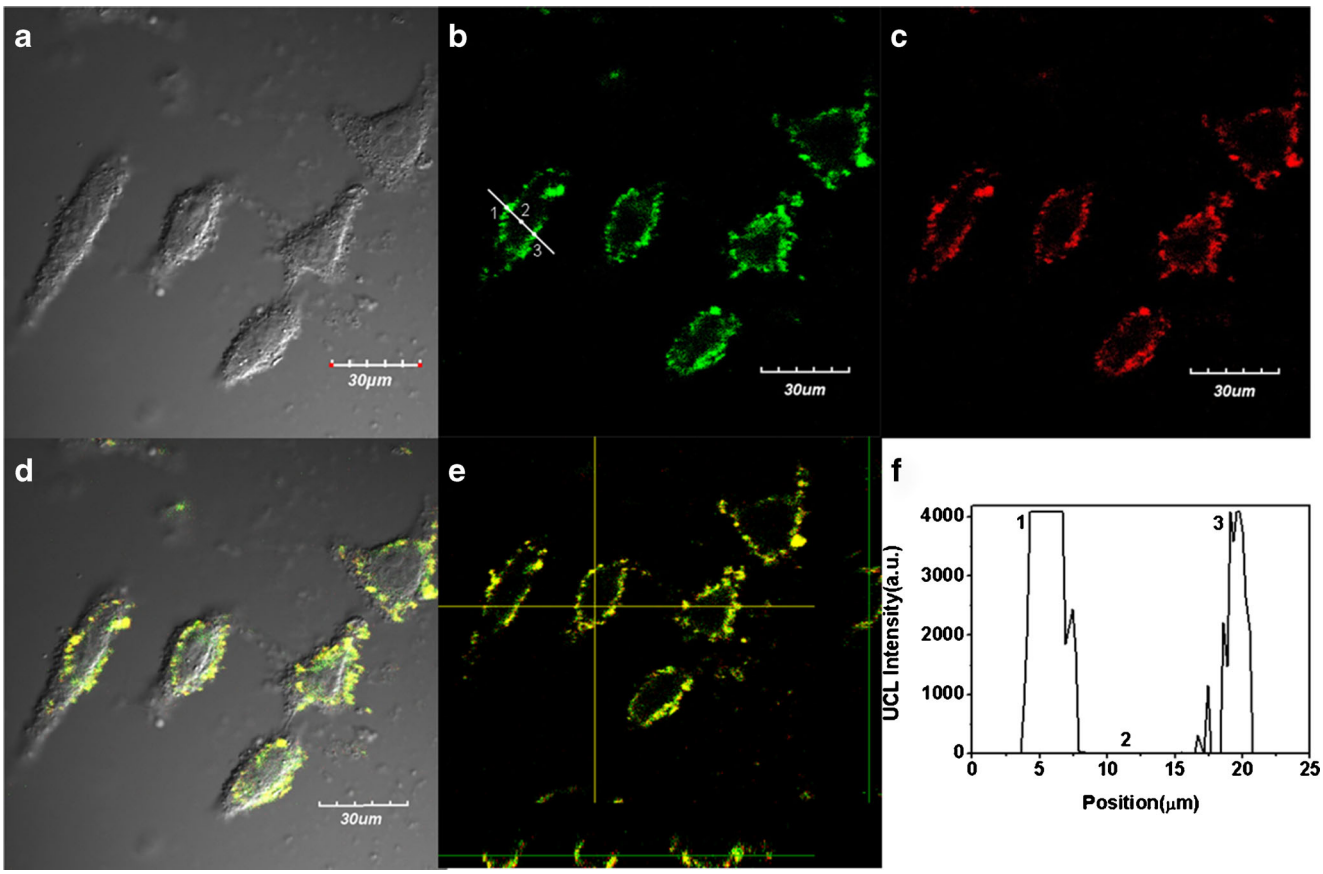

Fig. 5 Confocal imaging of KB cells incubated with MUCNs with a concentration of 200 $\mu g \cdot mL^{-1}$ for 1 h at 37 °C. (**a**) Bright-field image, (**b**) fluorescent images collected at *green* (520–560 nm) channels, (**c**) fluorescent images collected at *red* (630–670 nm) channels, (**d**) merged images of **a**, **b** and **c**, (**e**) three-dimensional confocal luminescent imaging, and (**f**) quantification analysis of UCL signal intensity along the *line* shown in **b** (inset) of a KB cell. (In region 1 and region 3, the counts are >4095; in region 2, the count is ~0)

Definitely, the laser scanning upconversion luminescence microscopy (LSUCLM) images [37] as shown in Fig. 5 ascertain the possibility mentioned above. The strong upconversion luminescent signals at 520–560 and 630–670 nm were observed from KB cells incubated with 200 $\mu g \cdot mL^{-1}$ serum-free medium containing MUCNs for 1 h at 37 °C. Overlays of LSUCLM images and bright-field images implied that the MUCNs had been endocytosed by cells rather than merely staining the membrane surface, which were further verified by three-dimensional luminescence images of live KB cells in Fig. 5e and confocal luminescence imaging data collected as a series along the Z-optical axis (Z-stack) (Fig. S5, ESI†).

Furthermore, quantification analysis of the UCL signal across the line (insert of Fig. 5b) reveals a perfect signal-to-noise ratio with extremely high UCL intensity surpassing the predetermined detection threshold (counts > 4095, region 1 and region 3) and no background fluorescence (counts ~0, region 2), as demonstrated in Fig. 5f, which suggests that the MUCNs are capable and promising biological luminescence labels for bioimaging without background fluorescence.

Conclusion

In summary, we have demonstrated an efficient one-step procedure to encapsulate monodisperse and hydrophobic UCNs within mesoporous silica directly, constructing water-soluable and uniform MUCNs ($NaYF_4$:Yb,Er@mSiO_2). MUCNs displayed good in vitro biocompatibility when incubated with KB cells even at the highest concentration according to an MTT assay. In particular, high-contrast in vitro bioimaging application certified the capability of MUCNs as biolabels upon 980 nm excitation. Moreover, this method provides the generality which can be extended to the meso-functionalization of other hydrophobic UCNs with different lanthanide doping and crystal shape for the preparation of multifunctional nanoparticles that can be further employed as drug delivery vehicle for simultaneous bioimaging and diagnosis. But before this happens, it is still challengeable to thoroughly understand the formation mechanism of mesoporous silica layer outside OA coated UCNs in ethanol and ammonia solution system. This work is ongoing in our group now.

Acknowledgments The authors are grateful to the financial support from the National Natural Science Foundation of China (Grant Nos. 21001072, 21231004), the Project-sponsored by SRF for ROCS, SEM., Innovation Program of Shanghai Municipal Education Commission (13ZZ073), the Key Subject of Shanghai Municipal Education Commission (J50102), and the project from State Key Laboratory of Rare Earth Resource Utilization (RERU2011012).

References

1. Lee JE, Lee N, Kim T, Kim J, Hyeon T (2011) Multifunctional mesoporous silica nanocomposite nanoparticles for theranostic applications. Acc Chem Res 44:893–902
2. Liu S, Chen G, Ohulchanskyy TY, Swihart MT, Prasad PN (2013) Facile synthesis and potential bioimaging application of hybrid upconverting and plasmonic $NaGdF_4$:Yb,Er-silica-gold nanoparticles. Theranostics. doi:10.7150/thno.4983
3. Wang F, Han Y, Lim CS, Lu Y, Wang J, Xu J, Chen H, Zhang C, Hong M, Liu XG (2010) Simultaneous phase and size control of upconversion nanocrystals through lanthanide doping. Nature 463: 1061–1065
4. Wang F, Deng R, Wang J, Wang Q, Han Y, Zhu H, Chen X, Liu XG (2011) Tuning upconversion through energy migration in core-shell nanoparticles. Nat Mater 10:968–973
5. Zou W, Visser C, Maduro JA, Pshenichnikov MS, Hummelen JC (2012) Broadband dye-sensitized upconversion of near-infrared light. Nat Photonics 6:560–564
6. Mader HS, Kele P, Saleh SM, Wolfbeis OS (2010) Upconverting luminescent nanoparticles for use in bioconjugation and bioimaging. Curr Opin Chem Biol 14:582–596
7. Wilhelm S, Hirsch T, Patterson WM, Scheucher E, Mayr T, Wolfbeis OS (2013) Protein-conjugatable multicolor upconversion nanoparticles. Theranostics. doi:10.7150/thno.5113
8. Zhu XJ, Zhou J, Chen M, Shi M, Feng W, Li FY (2012) Core-shell Fe3O4@NaLuF4:Yb, Er/Tm nanostructure for MRI, CT and upconversion luminescence tri-modality imaging. Biomaterials 33: 4618–4627
9. Yang YM, Zhao Q, Feng W, Li FY (2013) Luminescent chemodosimeters for bioimaging. Chem Rev 113:192–270
10. Liu JL, Liu Y, Liu Q, Li CY, Sun LN, Li FY (2011) Iridium(III) complex-coated nanosystem for ratiometric upconversion luminescence bioimaging of cyanide anions. J Am Chem Soc 133:15276–15279
11. Liu Q, Sun Y, Yang TS, Feng W, Li CG, Li FY (2011) Sub-10 nm hexagonal lanthanide-doped $NaLuF_4$ upconversion nanocrystals for sensitive bioimaging in vivo. J Am Chem Soc 133:17122–17125
12. Liu Q, Yang TS, Feng W, Li FY (2012) Blue-emissive upconversion nanoparticles for low-power-excited bioimaging in vivo. J Am Chem Soc 134:5390–5397
13. Idris NM, Gnanasammandhan MK, Zhang J, Ho PC, Mahendran R, Zhang Y (2012) In vivo photodynamic therapy using upconversion nanoparticles as remote-controlled nanotransducers. Nat Med 18: 1580–1585
14. Liu Q, Chen M, Sun Y, Chen GY, Yang TS, Gao Y, Zhang XZ, Li FY (2011) Multifunctional rare-earth self-assembled nanosystem for trimodal upconversion luminescence/fluorescence/positron emission tomography imaging. Biomaterials 32:8243–8253
15. Yang TS, Sun Y, Liu Q, Feng W, Yang P, Li FY (2012) Cubic sub-20 nm $NaLuF_4$-based upconversion nanophosphors for high-contrast bioimaging in different animal species. Biomaterials 33: 3733–3742
16. Gorelikov I, Matsuura N (2008) Single-step coating of mesoporous silica on cetyltrimethyl ammonium bromide-capped nanoparticles. Nano Lett 8:369–373
17. Kim J, Kim HS, Lee N, Kim T, Kim H, Yu T, Song IC, Moon WK, Hyeon T (2008) Multifunctional uniform nanoparticles composed of a magnetite nanocrystal core and a mesoporous silica shell for magnetic resonance and fluorescence imaging and for drug delivery. Angew Chem Int Ed 47:8438–8441
18. Deng YH, Qi DW, Deng CH, Zhang XM, Zhao DY (2008) Superparamagnetic high-magnetization microspheres with an Fe_3O_4@SiO_2 core and perpendicularly aligned mesoporous SiO_2 shell for removal of microcystins. J Am Chem Soc 130:28–29

19. Peng YK, Lai CW, Liu CL, Chen HC, Hsiao YH, Liu WL, Tang KC, Chi Y, Hsiao JK, Lim KE, Liao HE, Shyue JJ, Chou PT, Wolfbeis OS (2011) A new and facile method to prepare uniform hollow MnO functionalized $mSiO_2$ core shell nanocomposites. ACS Nano 5: 4177–4187
20. Wu SH, Hung Y, Mou CY (2011) Mesoporous silica nanoparticles as nanocarriers. Chem Commun 47:9972–9985
21. Qian HS, Guo HC, Ho PCL, Mahendran R, Zhang Y (2009) Mesoporous-silica-coated up-conversion fluorescent nanoparticles for photodynamic therapy. Small 5:2285–2290
22. Kang X, Cheng Z, Li C, Yang D, Shang M, Pa M, Li G, Liu N, Lin J (2011) Core–shell structured up-conversion luminescent and mesoporous $NaYF_4:Yb^{3+}/Er^{3+}@nSiO_2@mSiO_2$ nanospheres as carriers for drug delivery. J Phys Chem C 115:15801–15811
23. Yang JP, Deng YH, Wu QL, Zhou J, Bao HF, Li Q, Zhang F, Li FY, Tu B, Zhao DY (2010) Mesoporous silica encapsulating upconversion luminescence rare-earth fluoride nanorods for secondary excitation. Langmuir 26:8850–8856
24. Li CX, Liu JL, Alonso S, Li FY, Zhang Y (2012) Upconversion nanoparticles for sensitive and in-depth detection of Cu^{2+} ions. Nanoscale 4:6065–6071
25. Liu JN, Bu WB, Zhang SJ, Chen F, Xing HY, Pan LM, Zhou LP, Peng WJ, Shi JL (2012) Controlled synthesis of uniform and monodisperse upconversion core/mesoporous silica shell nanocomposites for bimodal imaging. Chem Eur J 18:2335–2341
26. Lim SF, Riehn R, Tung CK, Ryu WS, Zhuo R, Dalland J, Austin RH (2009) Upconverting nanophosphors for bioimaging. Nanotechnology 20:405701–405707
27. Chatterjee DK, Zhang Y (2012) Use of upconverting fluorescent nanoparticles for bioimaging. Proc SPIE 8272:827206. doi:10.1117/12.905939
28. Li CX, Hou ZY, Dai YL, Yang DM, Cheng ZY, Ma PA, Lin J (2013) A facile fabrication of upconversion luminescent and mesoporous core–shell structured β-$NaYF_4:Yb^{3+}$, $Er^{3+}@mSiO_2$ nanocomposite spheres for anti-cancer drug delivery and cell imaging. Biomater Sci 1:213–223
29. Gai SL, Yang PP, Li CX, Wang WX, Dai YL, Niu N, Lin J (2012) Synthesis of magnetic, up-conversion luminescent, and mesoporous core-shell-structured nanocomposites as drug carriers. Adv Funct Mater 20:1166–1172
30. Yang PP, Gai SL, Lin J (2012) Functionalized mesoporous silica materials for controlled drug delivery. Chem Soc Rev 41:3679–3698
31. Li ZQ, Zhang Y, Jiang S (2008) Multicolor core/shell-structured upconversion fluorescent nanoparticles. Adv Mater 20:4765–4769
32. Liu XM, Kong XG, Zhang YL, Tu LP, Wang Y, Zeng QH, Li CG, Shi Z, Zhang H (2011) Breakthrough in concentration quenching threshold of upconversion luminescence via spatial separation of the emitter doping area for bio-applications. Chem Commun 47: 11957–11959
33. Chen DQ, Lei L, Yang AP, Wang ZX, Wang YS (2012) Ultra-broadband near-infrared excitable upconversion core/shell nanocrystals. Chem Commun 48:5898–5900
34. Fan H, Yang K, Boye DM, Sigmon T, Malloy KJ, Xu H, López GP, Brinker CJ (2004) Self-assembly of ordered, robust, three-dimensional gold/silica nanocrystal arrays. Science 304:567–571
35. Liu Z, Sun LN, Li FY, Liu Q, Shi LY, Zhang DS, Yuan S, Liu T, Qiu YN (2011) One-pot self-assembly of multifunctional mesoporous nanoprobes with magnetic nanoparticles and hydrophobic upconversion nanocrystals. J Mater Chem 21:17615–17618
36. Zhou J, Liu Z, Li FY (2012) Upconversion nanophosphors for small-animal imaging. Chem Soc Rev 41:1323–1349
37. Sikora B, Fronc K, Kamińska I, Koper K, Szewczyk S, Paterczyk B, Wojciechowski T, Sobczak K, Minikayev R, Paszkowicz W, Stepien P, Elbaum D (2013) Transport of $NaYF_4:Er^{3+}$, Yb^{3+} upconverting nanoparticles into HeLa cells. Nanotechnology 24: 235702–235712